J. Fluid Mech. (1977), *vol.* 82, *part* 3, *pp.* 481–496
Printed in Great Britain

Grid turbulence near a moving wall

By N. H. THOMAS† AND P. E. HANCOCK
Department of Aeronautics, Imperial College, London

(Received 3 November 1976)

Decaying grid turbulence was passed over a wall moving at the stream speed. For the high Reynolds number of the experiment, the field due to the wall constraint on the normal component of the velocity fluctuations is found to extend further into the flow than the influence of the viscous boundary condition on the tangential-component fluctuations. Measurements of the variances, length scales and spectra of the three velocity components of the turbulence are compared with the results of a previous experiment and with the theoretical predictions for an idealization of the flow. A simple model for some departures from the theory is proposed.

1. Introduction

The experiment described below, in which decaying grid turbulence was passed over a wall moving at the stream speed, serves as a realization of the simplest bounded turbulence field: 'turbulence in a box'. For, invoking Taylor's frozen-flow hypothesis and supposing the grid turbulence to be essentially isotropic, we have an analogue of the boundary region established when an infinite flat plate is suddenly inserted, without relative mean motion, into a pre-existing field of homogeneous isotropic turbulence. Hunt & Graham (1978) have described the linearized asymptotic solution valid at large Reynolds number. Physically, this exhibits an outer kinematic region characterized by the length scale L_e of the external turbulence, in which the normal component of the velocity fluctuations is inhibited by the wall constraint, and an inner viscous region of typical thickness $\delta_v \sim (\nu t)^{\frac{1}{2}}$, where ν is the kinematic viscosity and t the elapsed time. The theory is valid for small δ_v/L_e.

The experiment, in which $t = x'/\overline{u}$, where x' is measured from the leading edge of the boundary region and $\overline{u}$ is the uniform mean velocity, affords a substantial test of the Hunt & Graham solution. We describe measurements of the time-averaged variances ($\overline{u'^2}$, $\overline{v'^2}$, $\overline{w'^2}$) of the fluctuation velocity components (u', v', w'), the one-dimensional frequency spectra ($\Theta_u, \Theta_v, \Theta_w$) of these components and the longitudinal integral scales defined by

$$L_u = \frac{\overline{u}}{4\overline{u'^2}}\Theta_u(n=0), \quad L_v = \frac{\overline{u}}{4\overline{v'^2}}\Theta_v(n=0), \quad L_w = \frac{\overline{u}}{4\overline{w'^2}}\Theta_w(n=0),$$

where n is the frequency. The subscript e will denote the values in the external stream. It is shown in § 3 that the normal ($\overline{v'^2}$) component is in quantitative agreement with the theory but the transverse ($\overline{w'^2}$) component is essentially uninfluenced by the wall, in

† Present address: Department of Applied Mathematics and Theoretical Physics, University of Cambridge.

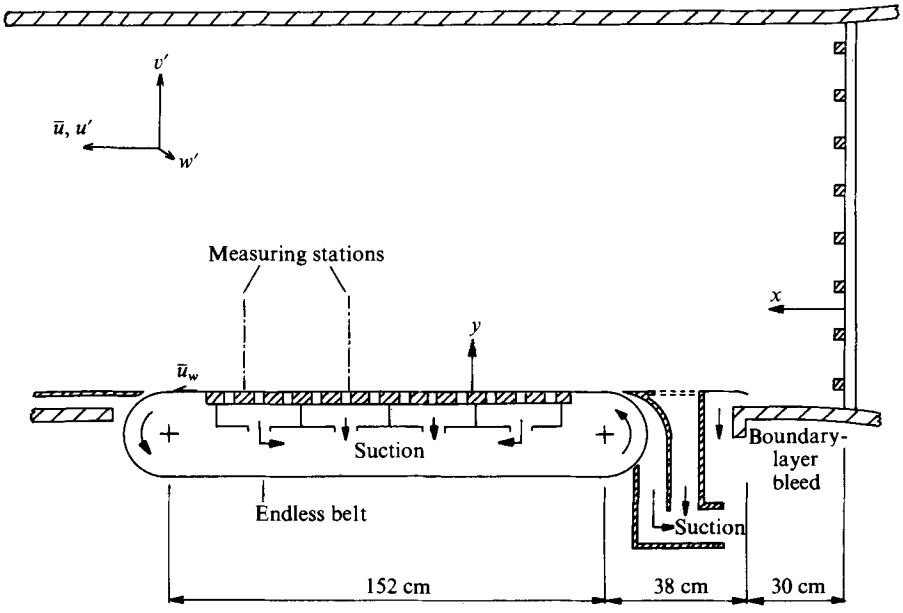

FIGURE 1. Schematic diagram of the wind tunnel, turbulence grid and endless belt arrangement, and definition sketch (the transverse co-ordinate z, not shown, has the centre-plane as origin).

contrast to the theoretically predicted amplification. The local amplification of the longitudinal ($\overline{u'^2}$) component, which is greater than that predicted, grows with increasing downstream distance. A simple explanation, in terms of the streamwise inhomogeneity of the decaying grid turbulence, is proposed in §4.

The present studies, in which the grid Reynolds number R_M was approximately 10^5, where $R_M = M\bar{u}/\nu$ and M is the mesh width, are complementary to those conducted by Uzkan & Reynolds (1967), in which R_M was about 5000. Essentially the same methods of producing a shear-free mean flow were employed (see §2). Uzkan & Reynolds measured the variance and spectrum of the u'-component fluctuation and found a viscous layer with $\delta_v \simeq 1{\cdot}8(\nu x'/\bar{u})^{\frac{1}{2}}$, but no explicit evidence for an outer kinematic region. Now, for large x/M, typically $L_{ue} \simeq 0{\cdot}1(Mx)^{\frac{1}{2}}$, where x is measured from the grid, so if $x \simeq x'$, then $\delta_v/L_{ue} \simeq (300/R_M)^{\frac{1}{2}}$ and is therefore approximately 0·25 for Uzkan & Reynolds' experiment and 0·05 for ours. Further discussion of Uzkan & Reynolds' results is presented in §4.

Hunt & Graham have compared their solution with the results of these moving-wall experiments and with measurements in a decaying turbulent stream by Graham (1975) and Petty (unpublished; see Hunt & Graham) near a flat plate and by Cooke (1971; see Hunt & Graham) near a wind-tunnel wall. Each study showed that outside the conventional mean-flow boundary layer, the v' variance decreased towards the wall as predicted by the theory. Graham's results, obtained near a mean-flow boundary layer of thickness small compared with L_{ue}, compare well with those currently obtained (see §3). This supports the view that, for a sufficiently high Reynolds number, the structure of the outer wall region is independent of the inner region even if the latter is a fully turbulent mean-flow boundary layer.

A practical application of the results is to the effects of free-stream turbulence on

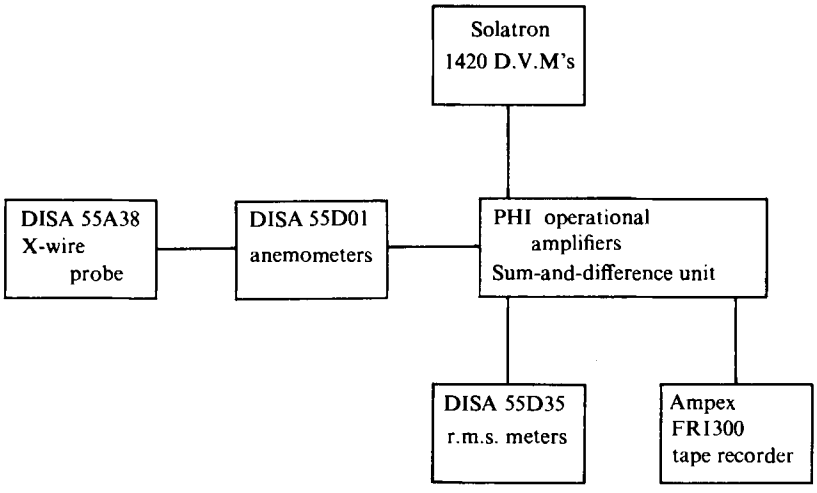

FIGURE 2. Apparatus for the collection and measurement of the turbulence data.

boundary layers when the free-stream length scale, as is usual, exceeds the boundary-layer thickness. In these cases, an outer kinematic region exists and the effective values of the turbulence parameters are not the external-stream values. Recent reviews of the problem of turbulent boundary layers with free-stream turbulence have been given by Green (1972) and Bradshaw (1974).

2. Procedure

The experiments were performed in a low-speed wind tunnel with a 5×4 ft ($1{\cdot}5 \times 1{\cdot}2$ m) working section 7 ft ($2{\cdot}1$ m) long, with corner fillets. The floor of the working section was replaced by an endless belt on rollers, with a suction-box assembly upstream (figure 1). The turbulence was generated by biplanar grids of rectangular-section bars with solidities of 0·4. The mesh widths were 3 in. (7·6 cm) and 6 in. (15·2 cm) respectively for the grids hereinafter referred to as grids A and B. The flow was studied at distances 168 cm and 193 cm downstream of grid A and 193 cm downstream of grid B. These stations are referred to below by their nominal downstream distances in grid mesh widths: $22M$, $25M$ and $13M$ respectively. A schematic diagram and definition sketch are shown in figure 1.

The belt, which was smooth except for a diagonal lap joint approximately 0·003 cm thick, was driven by a constant-speed motor at approximately 13 m s^{-1}. The belt speed was measured by a tachometer and also by a stroboscope focused on each roller; no slip was observed. A distribution of suction was applied through the backing plate to hold the belt flat. Frictional heating at this boundary generated a temperature rise of 8° C.

A bleed duct 30 cm downstream of the grid absorbed the tunnel boundary layer. The flow onto the moving belt was controlled by a leading-edge plate with suction through the porous surface and through the gap near the upstream roller (see figure 1). Using a tuft probe for visualization, the camber and incidence of the plate were adjusted to give smooth flow conditions. The size of the suction gap was set to minimize the mean shear at the downstream measurement station. This procedure may have

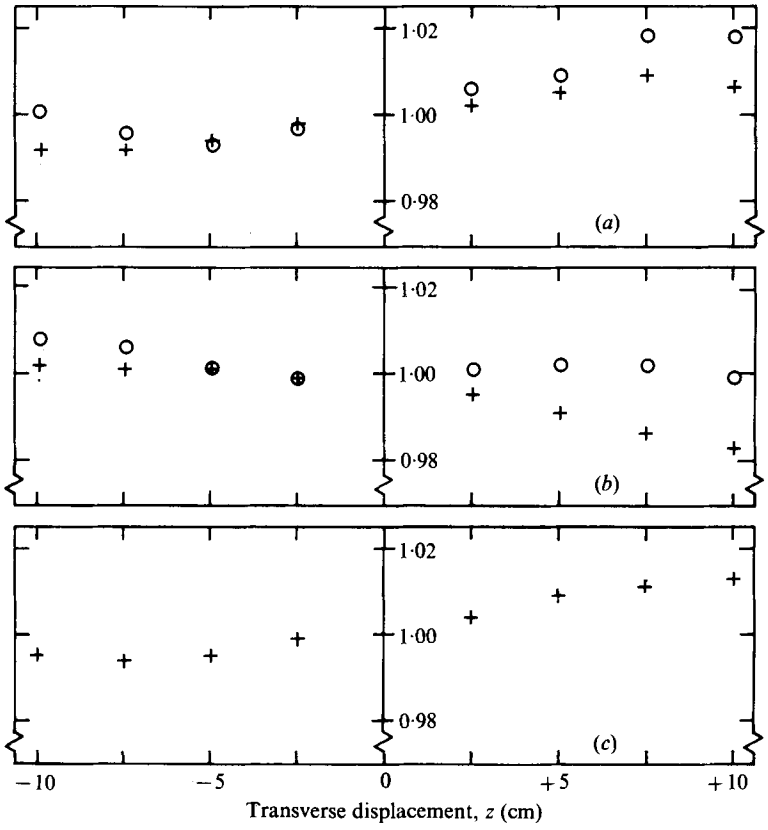

FIGURE 3. Transverse distributions of mean velocity normalized by values on $z = 0$. (*a*) $x/M = 25$, grid A ($M = 3$ in.). (*b*) $x/M = 13$, grid B ($M = 6$ in.). (*c*) $x/M = 22$, grid A. ○, $y = 0{\cdot}5$ cm; +, $y = 7{\cdot}6$ cm.

resulted in small differences in the configurations for the grid A study and the grid B study; the latter was performed at a later date.

The turbulence was measured by hot-wire anemometers. A diagram of the components is presented in figure 2. The probes were calibrated in the flow remote from the tunnel boundaries and 'best fit' King's law relations were used to derive the fluctuation velocities. The mean voltages of the two wires on a given cross-wire probe were matched over the calibration range and a sum-and-difference unit was employed to obtain fluctuating voltages proportional to the longitudinal and lateral components of the turbulence velocity fluctuations, assuming the wires angles to be $\pm 45°$. This assumption proved to be inadequate and corrections were later incorporated into the data reduction procedure; for details see Hancock & Thomas (1977).

The variances of the voltage fluctuations were measured by a commercial r.m.s. meter (figure 2). The recorded signals were later digitally sampled for 20 s at a rate of 2000 s^{-1} and Fourier transformed, using a fast algorithm described by Davies (1974), in blocks of 1024 samples. The effective 'filter' bandwidth was therefore 2 Hz and the total record length was 40 000 data points. No corrections for variations of the hot-wire sensitivities with spatial variations of air temperature were considered, but it was deduced from a comparison of the results of a Pitot-tube traverse and the mean voltage

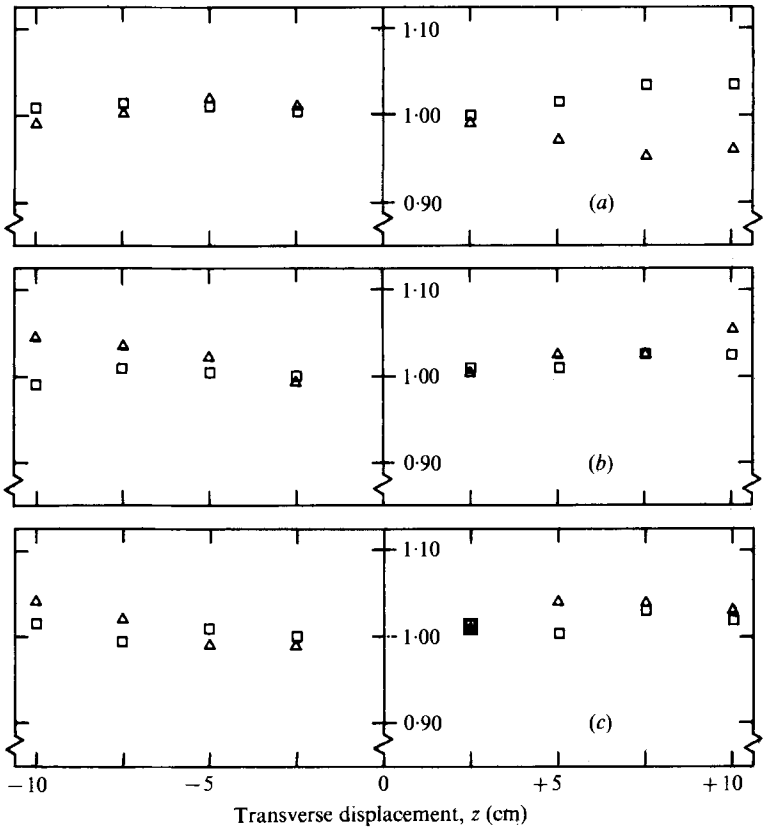

FIGURE 4. Transverse distributions of r.m.s. fluctuation velocities normalized by values on $z = 0$. (*a*) $x/M = 25$, $y = 0{\cdot}5$ cm. (*b*) $x/M = 25$, $y = 7{\cdot}6$ cm. (*c*) $x/M = 22$, $y = 7{\cdot}6$ cm. □, $(\overline{u'^2})^{\frac{1}{2}}$; △, $(\overline{v'^2})^{\frac{1}{2}}$.

outputs of the anemometers that any thermal boundary layer created by the temperature difference between the belt and the stream was essentially confined to a region closer to the wall than the data presented here.

3. Results

Any effects of the streamwise mean velocity variation, estimated as 0·1 % between the measuring stations, are assumed to be negligible. Transverse distributions of mean velocity at heights of 0·2 in. (0·5 cm) and 3 in. (7·6 cm) are shown in figure 3. Variations of less than ± 2 % over ± 10 cm are exhibited. Note that the necessary uniformity of speed at the wall does not suppress variations, presumably caused by the grid, at a height of 0·5 cm.

Figure 4 presents some transverse distributions of the r.m.s. values $(\overline{u'^2})^{\frac{1}{2}}$ and $(\overline{v'^2})^{\frac{1}{2}}$ of the u' and v' fluctuations for grid A only. Variations are typically less than 5 % over distances of ± 10 cm from the centre-plane. The differences between the distributions at heights of 0·5 cm and 7·6 cm at the $25M$ station may be due to a small inclination of the traverse relative to the wall.

Figure 5 shows mean velocity profiles obtained in the central plane at the $13M$ and $25M$ stations with minimized mean shear and with a nominal difference of ± 5 %

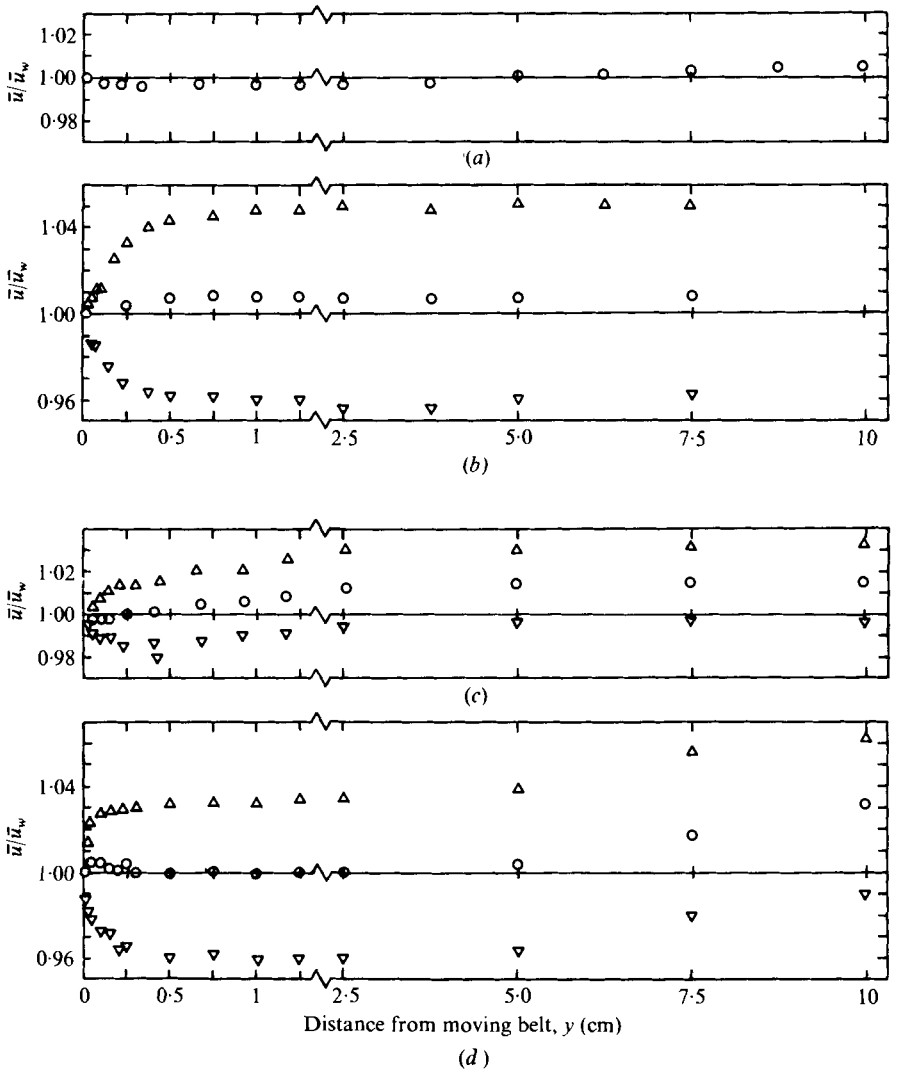

FIGURE 5. Mean velocity profiles at $x = 193$ cm showing the effects of a mismatch between the wall and stream speeds. Grid A experiment ($x/M = 25$): (*a*) without grid; (*b*) with grid. Grid B experiment ($x/M = 13$): (*c*) without grid; (*d*) with grid.

between the wall and stream speeds. For the experiment with grid A, the velocity is uniform to within 1% for $0 < y < 7{\cdot}5$ cm with the grid present and uniform to within $\frac{1}{2}$% for $0 < y < 10$ cm with the grid removed. For the grid B study, there is no significant gradient up to $y = 5$ cm but a 3% change between $y = 5$ cm and $y = 10$ cm. Here the measurement station is at only $13M$ and the gradient may well be due to grid-generated shear. With either grid in the tunnel, the wall shear field produced by deliberately mismatching the speed does not extend beyond $y \simeq 0{\cdot}5$ cm, which is in agreement with our earlier observation on the transverse non-uniformities.

Values of the r.m.s. velocity fluctuations obtained at the $25M$ station with the wall and stream speeds nominally equal and with a ± 5% mismatch between them are shown in figure 6. No significant differences between the three cases can be discerned

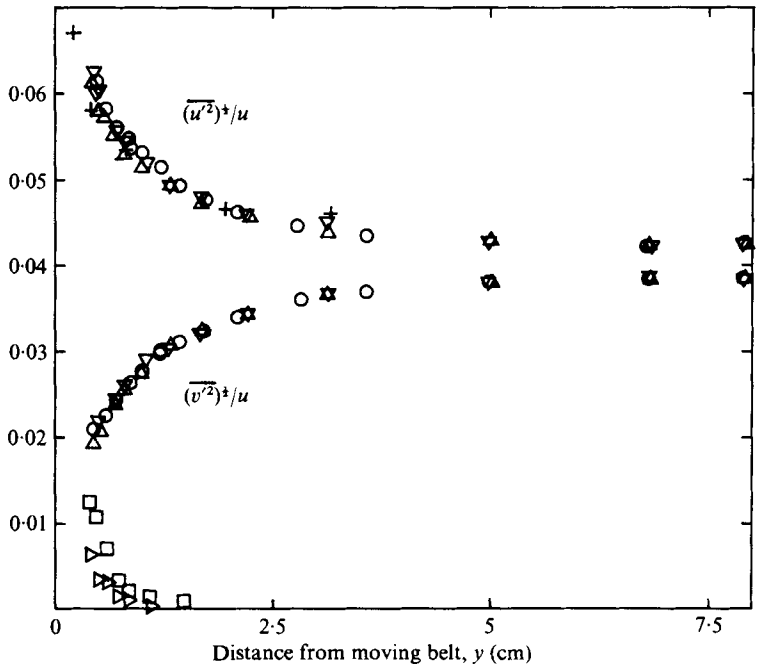

FIGURE 6. Turbulence intensities $(\overline{u'^2})^{\frac{1}{2}}/\bar{u}$ and $(\overline{v'^2})^{\frac{1}{2}}/\bar{u}$ at $x = 193$ cm. Grid A: ○, $\bar{u}_w = \bar{u}_e$; △, $\bar{u}_w = 0{\cdot}95\bar{u}_e$; ▽, $\bar{u}_w = 1{\cdot}05\bar{u}_e$; +, single-wire probe. No grid: □, $(\overline{u'^2})^{\frac{1}{2}}/\bar{u}$; ▷, $(\overline{v'^2})^{\frac{1}{2}}/\bar{u}$.

and we conclude that any influence on the turbulence is confined to the region of significant mean shear. Values of $(\overline{u'^2})^{\frac{1}{2}}$ obtained from a single wire agree to better than 5% with the cross-wire measurements. Figure 6 also shows the r.m.s.profiles obtained in the absence of the grid. This turbulence, probably generated near the leading edge, is presumably uncorrelated with the grid turbulence and contributes an error of less than about 5%.

Figure 7 presents the variances $(\overline{u'^2}, \overline{v'^2}, \overline{w'^2})$ normalized on their external-stream values $(\overline{u_e'^2}, \overline{v_e'^2}, \overline{w_e'^2})$ as functions of y/L_{ue}, where L_{ue} is the external longitudinal integral scale. The results for the normal $(\overline{v'^2})$ component correlate well and are supported by Graham's results for large-scale turbulence streaming past a flat-plate turbulent boundary layer. Figure 7 also shows the theoretical solution of Hunt & Graham. We observe that very good agreement is obtained if the reduced distance is based on the normal-component longitudinal integral scale L_{ve}, which was measured as $0{\cdot}4L_{ue}$ for the present grid turbulence rather than the value $0{\cdot}5L_{ue}$ for the isotropic field assumed in the analysis. Over the range of heights used in the present study, the transverse $(\overline{w'^2})$ component varies only slightly towards the wall, the variation decreasing with downstream distance. Hunt & Graham's solution for homogeneous isotropic external turbulence considerably overpredicts the values near the wall. The longitudinal $(\overline{u'^2})$ component increases towards the wall, the amplification growing significantly with downstream distance. The results at $13M$ are in reasonable agreement with the theory but local scaling is clearly inadequate for a description of the downstream evolution. Further discussion of this behaviour will be given in §4.

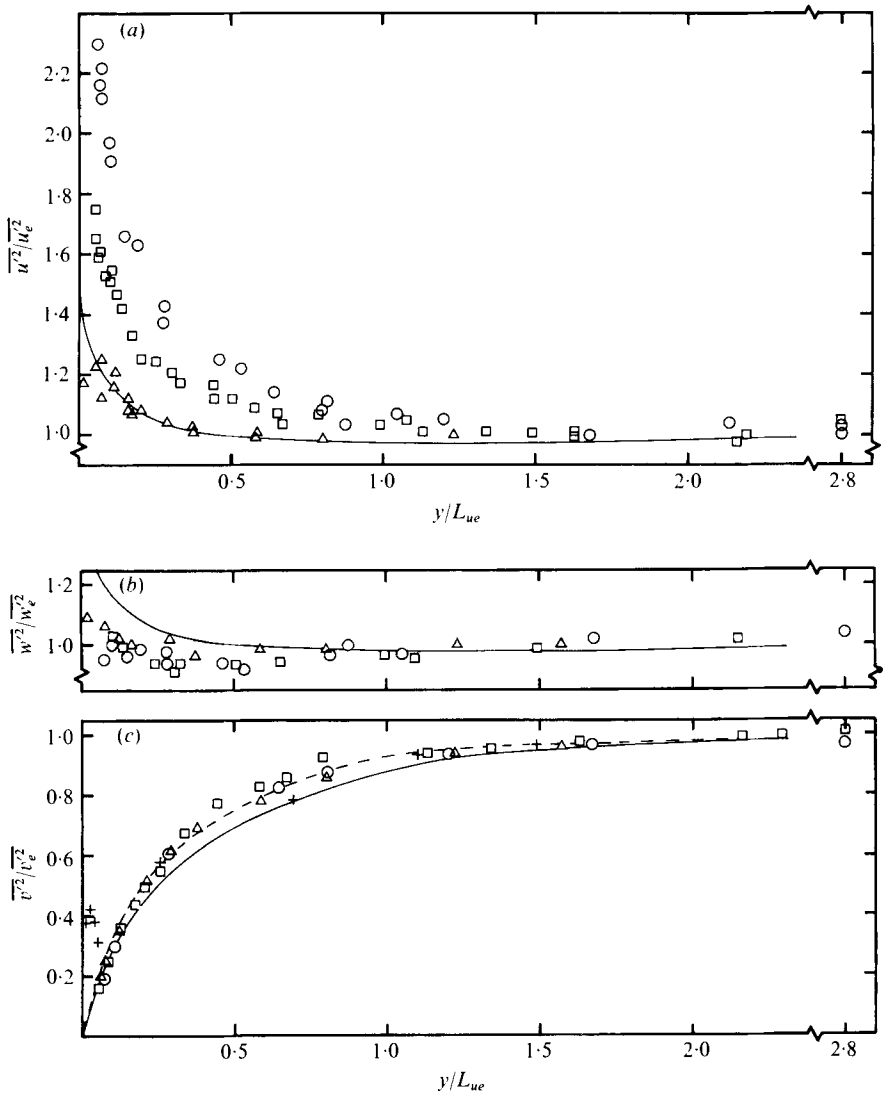

FIGURE 7. Variances of fluctuation velocities normalized on external-stream values as functions of y/L_{ue}. (*a*) $\overline{u'^2}/\overline{u_e'^2}$. (*b*) $\overline{w'^2}/\overline{w_e'^2}$. (*c*) $\overline{v'^2}/\overline{v_e'^2}$. △, $x/M = 13$, $(\overline{u_e'^2})^{\frac{1}{2}}/\bar{u} = 0{\cdot}0775$, $(\overline{w_e'^2})^{\frac{1}{2}}/\bar{u} = 0{\cdot}0700$, $(\overline{v_e'^2})^{\frac{1}{2}}/\bar{u} = 0{\cdot}0700$; □, $x/M = 22$, $(\overline{u_e'^2})^{\frac{1}{2}}/\bar{u} = 0{\cdot}0525$, $(\overline{w_e'^2})^{\frac{1}{2}}/\bar{u} = 0{\cdot}0483$, $(\overline{v_e'^2})^{\frac{1}{2}}/\bar{u} = 0{\cdot}0483$; ○, $x/M = 25$, $(\overline{u_e'^2})^{\frac{1}{2}}/\bar{u} = 0{\cdot}0425$, $(\overline{w_e'^2})^{\frac{1}{2}}/\bar{u} = 0{\cdot}0380$, $(\overline{v_e'^2})^{\frac{1}{2}}/\bar{u} = 0{\cdot}0380$; +, experiment of Graham (1975); ——, theory of Hunt & Graham (1978); – – –, $\overline{v'^2}/\overline{v_e'^2}$ *vs.* $0{\cdot}4y/L_{ve}$.

Length-scale profiles derived from the frequency spectra are shown in figure 8. The scatter hides any trends with downstream distance. The normal-component length scale L_v decreases monotonically towards the wall and appears to extrapolate to zero at the wall, in agreement with the theoretical solution. The transverse-component length scale L_w increases to a measured maximum amplification of 1·6 times the external value at the measurement position nearest the wall. This is consistent with the theory, which predicts a wall scale of twice the external-stream value. The longitudinal-component length scale L_u appears to rise slightly (5 %), then decreases monotonically

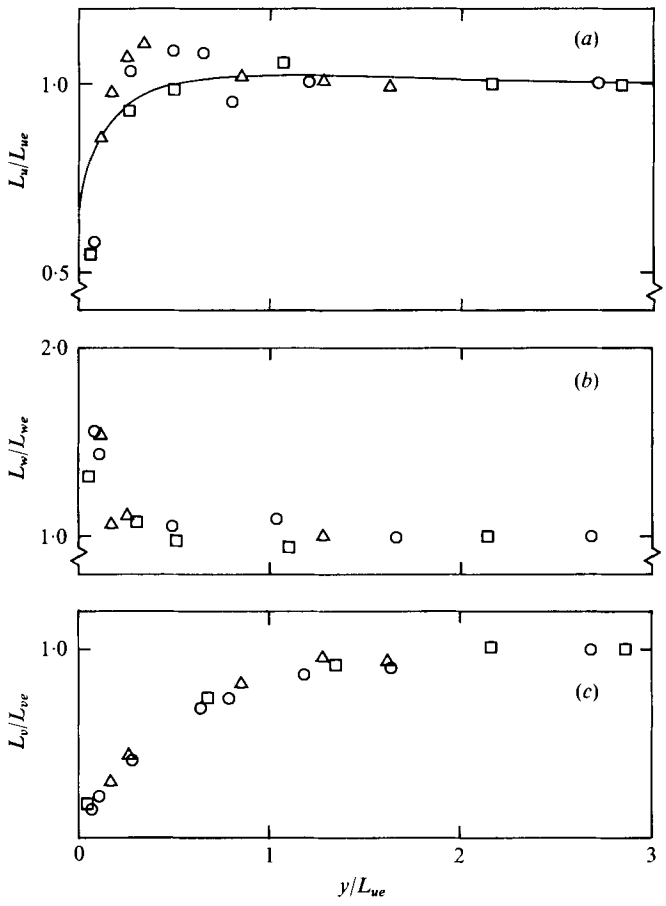

FIGURE 8. Longitudinal integral scales normalized on external-stream values as functions of y/L_{ue}. (*a*) L_u/L_{ue}. (*b*) L_w/L_{we}. (*c*) L_v/L_{ve}. △, $x/M = 13$, $L_{ue}/M = 0{\cdot}393$, $L_{we}/M = 0{\cdot}157$, $L_{ve}/M = 0{\cdot}157$; □, $x/M = 22$, $L_{ue}/M = 0{\cdot}583$, $L_{we}/M = 0{\cdot}233$, $L_{ve}/M = 0{\cdot}233$; ○, $x/M = 25$, $L_{ue}/M = 0{\cdot}633$, $L_{we}/M = 0{\cdot}253$, $L_{ve}/M = 0{\cdot}253$; ——, theory of Hunt & Graham (1978).

to a measured minimum of $0{\cdot}5\,L_{ue}$. The theoretical result is shown to be in reasonable agreement for $y/L_{ue} > 0{\cdot}1$ but the theoretical value at the wall is $\frac{2}{3}L_{ue}$.

One-dimensional frequency spectra are displayed in figure 9. In agreement with the theory, the high frequency ranges are relatively unaffected by the presence of the wall, with the exception of the longitudinal component within an inner region of thickness approximately $0{\cdot}25L_{ue}$, where the energy density grows towards the wall and increases with downstream distance. The dominant characteristic of the low frequency range is the decrease in the normal-component energy towards the wall, which is in good agreement with the theoretical solution. The gain in low frequency energy density of the transverse component also conforms with the theory, but the reduction found in the intermediate frequency range is not predicted. The low frequency energy density of the longitudinal component increases towards the wall and then decreases within the inner region referred to above, while the theoretical solution predicts the low frequency asymptote to be independent of the normal distance y. The results at $13M$ generally support the theory.

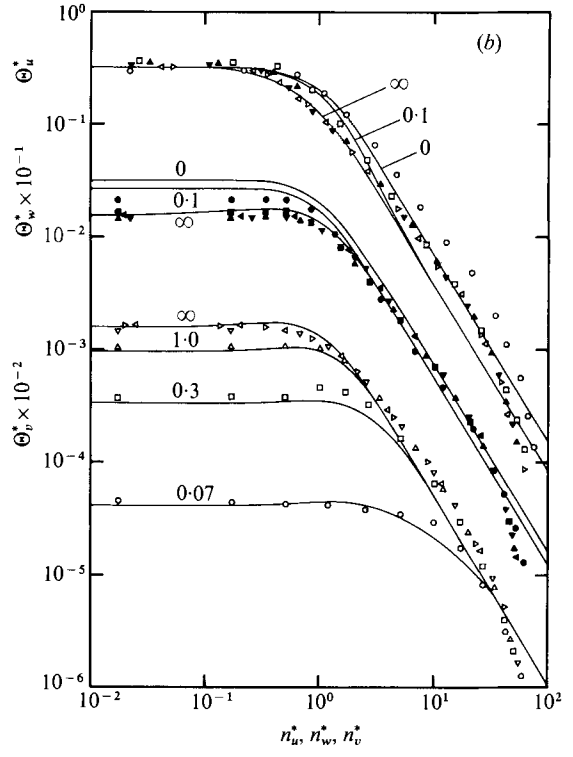

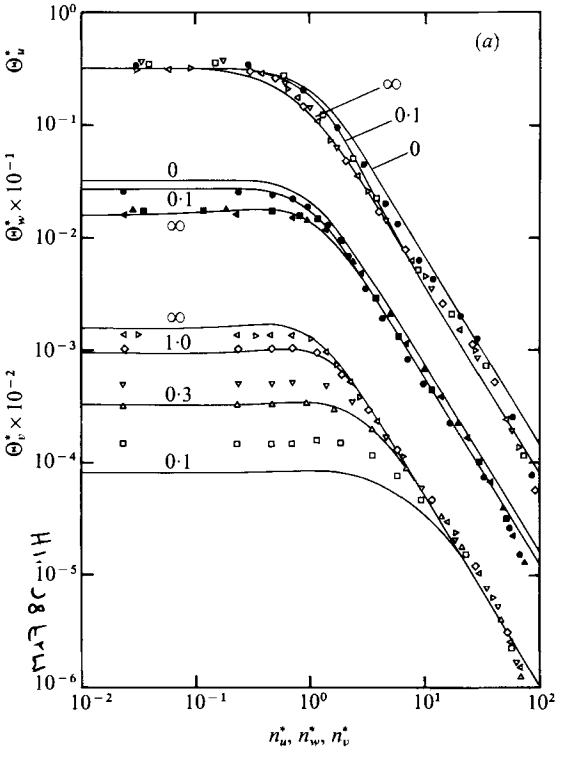

FIGURES 9(*a*) and (*b*). For legend see next page.

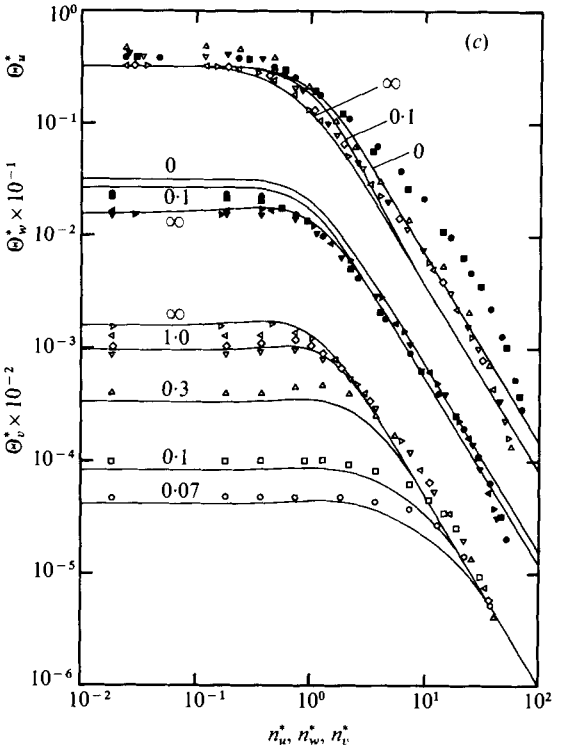

FIGURE 9. Normalized frequency spectra

$$\Theta_u^* = \bar{u}\Theta_u/4\pi u_e'^2 L_{ue}, \quad \Theta_w^* = \bar{u}\Theta_w/8\pi\overline{w_e'^2} L_{we}, \quad \Theta_v^* = \bar{u}\Theta_v/8\pi\overline{v_e'^2} L_{ve}$$

as functions of the normalized frequencies

$$n_u^* = 2\pi n L_{ue}/\bar{u}, \quad n_w^* = 4\pi n L_{we}/\bar{u}, \quad n_v^* = 4\pi n L_{ve}/\bar{u} \text{ respectively.}$$

(*a*) $x/M = 13$. (*b*) $x/M = 22$. (*c*) $x/M = 25$. ——, theory of Hunt & Graham (1978).

	○	□	△	▽	◇	◁	▷	●	■	▲	▼	◀	▶
y/L_{ue} (*a*)		0·166	0·255	0·340	0·851	1·28	1·63	0·111	0·170	0·251		1·28	
(*b*)	0·057	0·256	0·674	1·34		2·16	2·84	0·057	0·297	0·506	1·09	2·14	
(*c*)	0·047	0·107	0·283	0·647	0·802	1·20	2·78	0·080	0·102		0·497	1·05	2·73

4. Discussion

The present configuration, in contrast to that used by Uzkan & Reynolds, has a bleed duct upstream of the moving wall and this ensures removal of any 'horseshoe' trailing vortex structures arising where the tunnel boundary layer flows between the bars of the grid. Uzkan & Reynolds' measurements do not establish the degree of uniformity of the mean flow close to the surface at the downstream study stations. Cooke's measurements near a wind-tunnel wall may also have been influenced by the presence of horseshoe vortices. On the other hand, the present arrangement may have introduced some small streamline curvature in the entry zone and an associated turbulence distortion field. No flow measurements were taken in this region but the short entry length, the tuft-probe observations and the low turbulence levels obtained at the measuring stations in the absence of the grids suggest that any downstream influence

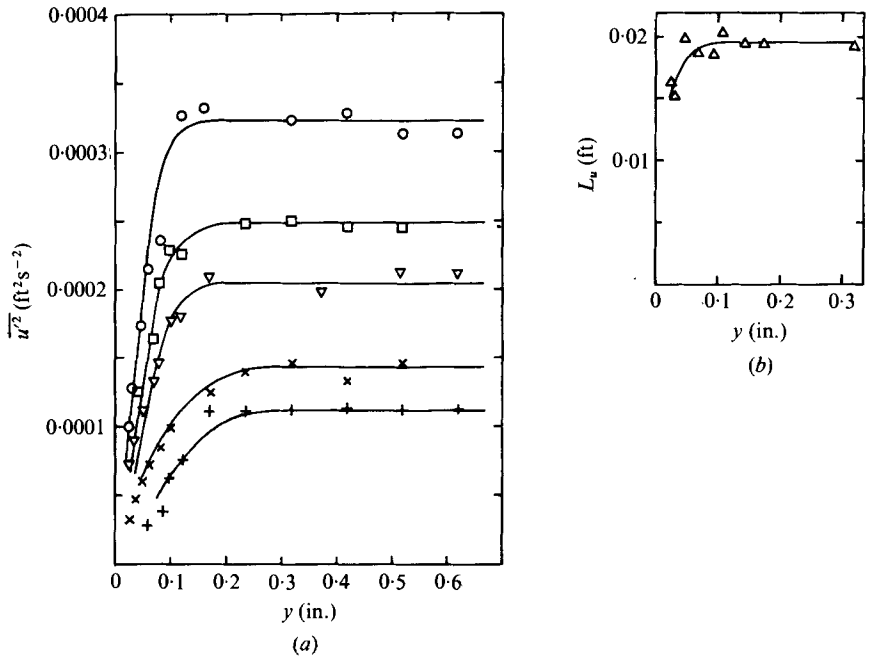

FIGURE 10. Turbulence measurements by Uzkan & Reynolds (1967). (*a*) $\overline{u'^2}$ (from Uzkan & Reynolds 1967, figure 13). $\bar{u} = 0{\cdot}315\,\mathrm{ft\,s^{-1}}$: ○, $x/M = 7{\cdot}5$; ▽, 12·5; ×, 15·0; +, 17·5. $\bar{u} = 0{\cdot}330$ ft s^{-1}: □, $x/M = 11{\cdot}5$. (*b*) L_u (from Uzkan & Reynolds 1967, figure 18): △, $x/M = 7{\cdot}5$.

is negligible. Graham's and Petty's measurements near a flat plate are subject to similar uncertainties about the downstream effects of distortion near the leading edge.

Uzkan & Reynolds presented variances, scales and spectra of the longitudinal component obtained in a nominally shear-free water flow at a mesh Reynolds number $R_M \simeq 5000$. Figure 10 reproduces their figure 13 (with the abscissa scale corrected for misprints) and their figure 18. In contrast to the present results, the $\overline{u'^2}$-component profiles decline monotonically towards the wall. Uzkan & Reynolds took this as confirmation of a satisfactory matching of the wall and stream speeds and inferred a viscous scaling for the wall layer, with thickness $\delta_v \simeq 1{\cdot}8(x'\nu/\bar{u})^{\frac{1}{2}}$, where x' is measured from the start of the layer. Their integral-scale profile is comparable with those currently obtained but the absolute values appear to be small, giving $L_{ue}/M \simeq 0{\cdot}12$. An expected value obtained from the survey of Naudascher & Farrell (1970) and giving $L_{ue}/M \simeq 0{\cdot}4$ at $x/M = 16$ indicates that for Uzkan & Reynolds' study $\delta_v/L_{ue} \simeq 0{\cdot}25$. The current results have shown that the total wall-layer thickness is approximately $2L_{ue}$, so it appears that for Uzkan & Reynolds' experiment there was, as they suggested, a substantial outer kinematic field. Using the above expression for δ_v, we find that in the present experiment, in which R_M was approximately 20 times Uzkan & Reynolds' value, $\delta_v/L_{ue} \simeq 0{\cdot}05$. This implies that all our measurements were taken outside the viscous layer, which is consistent with the results obtained. Hunt & Graham discussed a generally successful reconciliation of the two sets of results with arguments stemming from their two-layer analysis. However, their solution does not adequately describe the evolution of the u' component observed in the present experiment, and we now consider this development.

In the absence of gradients of mean velocity, the Reynolds mean momentum equations are

$$\frac{\partial}{\partial x}(\bar{p}+\overline{u'^2})+\frac{\partial}{\partial y}\overline{u'v'}=0, \quad \frac{\partial}{\partial y}(\bar{p}+\overline{v'^2})+\frac{\partial}{\partial x}\overline{u'v'}=0,$$

where $\bar{p}$ is the 'kinematic' pressure. Noting that the spatial derivatives $\partial/\partial x$ and $\partial/\partial y$ operating on the time-averaged variables are of orders $[(\overline{u'^2})^{\frac{1}{2}}/\bar{u}]\ L_{ue}^{-1}$ and L_{ue}^{-1} and neglecting terms $O(\overline{u'^2}/\bar{u}^2)$, these equations may be combined to give

$$\frac{\partial}{\partial x}(\overline{u'^2}-\overline{v'^2})+\frac{\partial}{\partial y}\overline{u'v'}=\frac{\partial}{\partial x}(\overline{u_e'^2}-\overline{v_e'^2}).$$

It is easily demonstrated that this equation holds for any irrotational mean velocity field. However, without additional information it merely relates three components of the Reynolds-stress tensor. Values of $\overline{u'v'}$ calculated from the current experimental data were found to be too small to be reliable. We adopt the strategy of assuming a sufficiently large Reynolds number $Re = (\overline{u_e'^2})^{\frac{1}{2}} L_{ue}/\nu$ for validity of Hunt & Graham's solution for the v' component, which is supported by the present results, and then consider the implied limiting responses of $\overline{u'^2}$ and $\overline{u'v'}$. This essentially heuristic procedure indicates a plausible closure equation for $\overline{u'v'}$ in terms of the known $\overline{v'^2}$ field, with magnitude dependent on Re; the latter is presumably the dominant parameter distinguishing Uzkan & Reynolds' experiment from the present one. We can then calculate the implied evolution of the $\overline{u'^2}$ field.

The continuity equation suggests that $(\overline{v'^2})^{\frac{1}{2}}(y=\delta_v) \sim \delta_v(\overline{u_e'^2})^{\frac{1}{2}}/L_{ue}$, so for a substantial outer region it is necessary that $\delta_v/L_{ue} \ll 1$ and for the v' field to be essentially kinematic everywhere, $(\overline{u_e'^2})^{\frac{1}{2}}\delta^2/\nu L_{ue} \gg 1$, or $Re\,(\delta_v/L_{ue})^2 \gg 1$. Uzkan & Reynolds' experimental results show $\delta_v/L_{ue} \simeq 0{\cdot}25$ at $Re \simeq 100$, while the present experiment with grid A gives $\delta_v/L_{ue} \simeq 0{\cdot}05$ at $Re \simeq 2000$ and that with grid B gives $\delta_v/L_{ue} \simeq 0{\cdot}04$ at $Re \simeq 4000$. It appears that for all the experiments $\delta_v/L_{ue} \simeq (6/Re)^{\frac{1}{2}}$.

If $\overline{u'v'}$ is sufficiently small for the approximation

$$\frac{\partial}{\partial x}(\overline{u'^2}-\overline{u_e'^2})=\frac{\partial}{\partial x}(\overline{v'^2}-\overline{v_e'^2})$$

to be valid then the decay rate of $\overline{u'^2}$ is reduced near the wall, which is consistent with the present results. On the other hand, Uzkan & Reynolds' results for the outer region show $\overline{u'^2} \simeq \overline{u_e'^2}$, in which case the equation approximates to

$$\frac{\partial}{\partial y}\overline{u'v'}=\frac{\partial}{\partial x}(\overline{v'^2}-\overline{v_e'^2}).$$

Taking both these limits into consideration, we propose as a closure equation

$$\frac{\partial}{\partial y}\overline{u'v'}=f(Re)\frac{\partial}{\partial x}(\overline{v'^2}-\overline{v_e'^2}),$$

where $f(Re \to \infty) \to 0$ and $f(Re \simeq 100) \simeq 1$. For an estimation of the form of $f(Re)$, we assume a viscous scale for $\overline{u'v'}$ given by $(\overline{u'^2v'^2})^{\frac{1}{2}}(y=\delta_v) \simeq \overline{u_e'^2}\,\delta_v/L_{ue}$, which is proportional to $Re^{-\frac{1}{2}}\overline{u_e'^2}$. This suggests that the magnitude of $\overline{u'v'}$ is an order smaller than in a fully turbulent shear layer and so accounts for the unreliability of the present

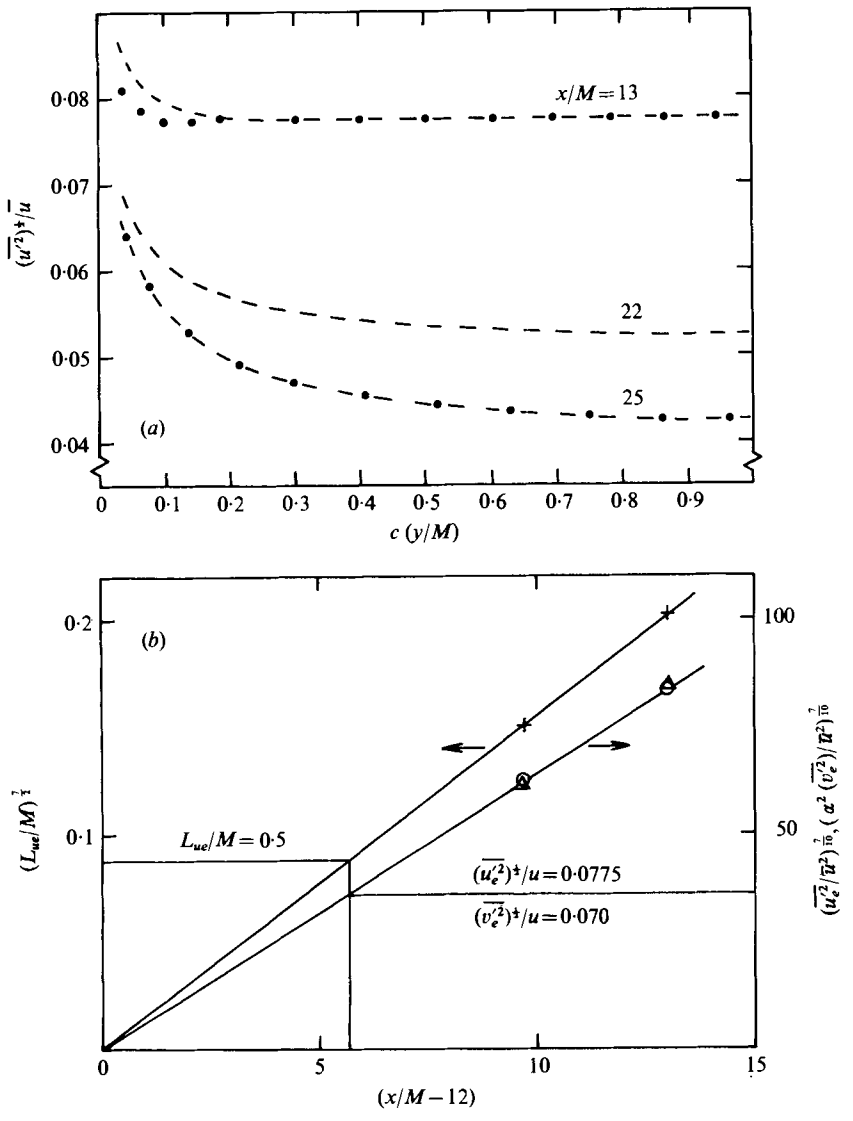

FIGURE 11. (*a*) Turbulence intensity $(\overline{u'^2})^{\frac{1}{2}}/\bar{u}$: ●, calculated from the model equation; – –, experimental values; $c = 1$ for grid A, $c = (L_{ue}/M)_A (L_{ue}/M)_B^{-1}$ for grid B. (*b*) Energy decay and length-scale growth for the turbulence generated by grid A compared with the Kolmogorov '$\frac{10}{7}$' decay law: ○, $\overline{u_e'^2}/\bar{u}^2$; △, $\overline{v_e'^2}/\bar{u}^2$; $\alpha = (\overline{u_e'^2}/\overline{v_e'^2})^{\frac{1}{2}} = 1·11$.

experimental values. The assumed scaling indicates that an appropriate choice is $f \propto Re^{-\frac{1}{2}}$ and substitution in the closure proposal yields

$$\frac{\partial}{\partial y}\overline{u'v'} \simeq 10Re^{-\frac{1}{2}}\frac{\partial}{\partial x}(\overline{v'^2} - \overline{v_e'^2}).$$

Figure 11 (*a*) shows the calculated values of $(\overline{u'^2})^{\frac{1}{2}}/\bar{u}$ at $x/M = 25$ for $Re = 2000$ obtained using the faired experimental profile at $x/M = 22$ as the initial curve. Excellent agreement with the experimental results is demonstrated. Figure 11 (*b*) shows

that, in the external stream, the variances and the length scales of the turbulence generated by grid A are described near the test stations by the Kolmogorov '$\frac{10}{7}$' energy decay law (Comte-Bellot & Corrsin 1966) with a single virtual origin at $x/M \simeq 12$. Extrapolation suggests that the external-stream variances found at $x/M = 13$ with grid B would be obtained at $x/M = 18$ with grid A and that the length scale would be $0{\cdot}5M$. As a further test of the model, figure 11(*a*) shows the inferred profile at $x/M = 18$ calculated from the data at $x/M = 22$, and the experimental results obtained with grid B. The normal co-ordinate y has been stretched in an effort to accommodate the different length scales. Although a comparison is not strictly admissible, the model follows the experimental trends: the amplification and the boundary-region thickness of the u' component are reduced.

The u'-component spectra demonstrated that the transferred energy resides in the intermediate and high frequency ranges. A reduction of this energy with decreasing Re, as supposed in the model, is consistent with these spectral observations. The model does not explain the departures from the theory of the w' component, but the spectra showed that these occur mainly in the intermediate and high frequency ranges, so they may be related to the development of the u' component.

5. Conclusions

At high Reynolds numbers, the outer region of a turbulent boundary region with zero mean shear scales on the external turbulence parameters. The normal fluctuating component is inhibited within a layer of characteristic thickness about twice the external longitudinal integral length scale. The profiles of this component are in good agreement with the theoretical solution given by Hunt & Graham. The amplification of the longitudinal component is also in accordance with the theory and in marked contrast to the essentially viscous response observed by Uzkan & Reynolds at about one-tenth of the present mesh Reynolds number. In terms of the microscale Reynolds number $R_\lambda = (\overline{u_e'^2})^{\frac{1}{2}} \lambda/\nu$, the present experiment, with $R_\lambda \simeq 120$, as opposed to Uzkan & Reynolds' experiment, with $R_\lambda \simeq 25$, should be typical of all high Reynolds number flows, with $R_\lambda > 100$, say. The longitudinal component shows a downstream development not predicted by the theory but plausibly described by a model of the dynamical equation incorporating Uzkan & Reynolds' experimental results. The lateral component appears to be only weakly influenced by the wall and its behaviour remains to be explained.

The integral length scales of the three fluctuating components are generally in agreement with the theoretical solution, with the exception of the longitudinal component near the wall. The latter is smaller than is predicted.

The spectra tend to confirm the *prima facie* expectation that the smaller eddies will be less influenced by the wall than the larger ones. The normal-component spectra are in good agreement with the theory. The increase in the longitudinal-component variance is associated with the intermediate and higher frequency ranges, as is the reduced variance of the lateral component. The generally reasonable agreement in the low frequency ranges is satisfying since the premises of the theory, such as second-order weak interactions, are more adequately met.

We are grateful to Dr P. W. Bearman and Mr P. Bradshaw for their valuable advice during this study. Acknowledgement is made to the Science Research Council, who supported this work. P. E. Hancock was in receipt of a Science Research Council maintenance grant.

REFERENCES

BRADSHAW, P. 1974 Effects of free-stream turbulence on turbulent shear layers. *Imperial College Aero. Rep.* no. 74-10.

COMTE-BELLOT, G. & CORRSIN, S. 1966 The use of a contraction to improve the isotropy of grid-generated turbulence. *J. Fluid Mech.* **25**, 657.

DAVIES, M. E. 1974 Spectral analysis programs Powspec and Cophase. *Imperial College Aero. Tech. Note* no. 74-103.

GRAHAM, J. M. R. 1975 Turbulent flow past a long flat plate. *Imperial College Aero. Tech. Note* no. 75–101.

GREEN, J. E. 1972 On the influence of free stream turbulence on a turbulent boundary layer as it relates to wind tunnel testing at subsonic speeds. *R.A.E. Tech. Rep.* no. 72201.

HANCOCK, P. E. & THOMAS, N. H. 1977 Grid turbulence near a moving wall. *Imperial College Aero. Note* (to be published).

HUNT, J. C. R. & GRAHAM, J. M. R. 1978 Free-stream turbulence near plane boundaries. To be published.

NAUDASCHER, E. & FARELL, C. 1970 Unified analysis of grid turbulence. *Trans. A.S.C.E.* **96** (EM2), 121.

UZKAN, T. & REYNOLDS, W. C. 1967 A shear-free turbulent boundary layer. *J. Fluid Mech.* **28**, 803.